

# Table Detection in the Wild: A Novel Diverse Table Detection Dataset and Method

Mrinal Haloi, Shashank Shekhar, Nikhil Fande, Siddhant Swaroop Dash, Sanjay G  
Subex AI Labs

Email: mrinalhaloi11@gmail.com, shashekharank@gmail.com

**Abstract**—Recent deep learning approaches in table detection achieved outstanding performance and proved to be effective in identifying document layouts. Currently, available table detection benchmarks have many limitations, including the lack of samples diversity, simple table structure, the lack of training cases, and samples quality. In this paper, we introduce a diverse large-scale dataset for table detection with more than seven thousand samples containing a wide variety of table structures collected from many diverse sources. In addition to that, we also present baseline results using a convolutional neural network-based method to detect table structure in documents. Experimental results show the superiority of applying convolutional deep learning methods over classical computer vision-based methods. The introduction of this diverse table detection dataset will enable the community to develop high throughput deep learning methods for understanding document layout and tabular data processing.

Dataset is available at: 1. <https://www.kaggle.com/datasets/mrinalim/stdw-dataset>

2. <https://huggingface.co/datasets/n3011/STDW>

## I. INTRODUCTION

Table detection is one of the crucial tasks in document layout analysis and table data understanding. Especially for extracting data from scanned documents table detection plays a significant role.

The recent development of applying deep learning in computer vision-related tasks enabled the researcher to develop a state-of-the-art document layout analysis system [1, 2]. Deep learning technique such as convolutional neural network is widely used in segmentation [3], classification [4, 5] and object detection task [6]. Building a high-performance convolutional model requires a large dataset resembling the target problem. A good dataset has the attributes of good samples diversity, high-quality ground truths, readable samples resolution, and a lot of training cases. As we have observed, all the current table detection datasets have various limiting aspects.

Firstly, the quality of samples available in these datasets is not adequate, which makes it hard for the trained model to generalize well in the high-quality sample cases. The structural details of tables are important in the detection and low-quality samples lack clarity in capturing minute details of tables structure. Hence, samples resolution and quality are important in the training detection model.

Secondly, the diversity of samples is very limited. Dataset samples should capture all possible variations of table structures starting from a simple table to complex nested table structures including grid and non-grid variations. Deep learn-

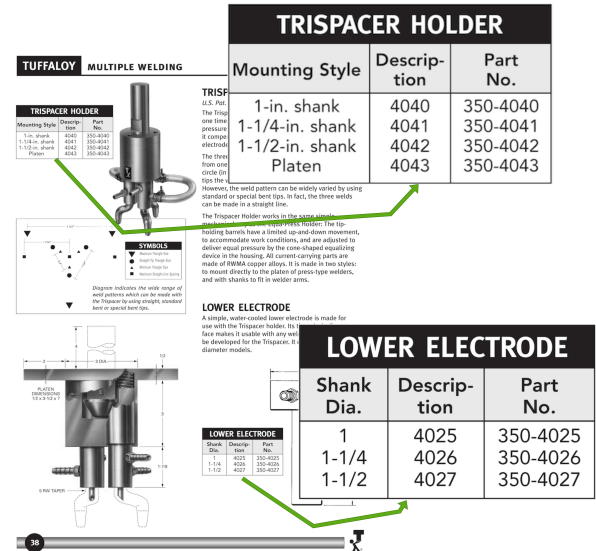


Fig. 1. Table detection in documents. An example of tables in a datasheet document.

ing model generalization performance improves with diverse discriminative samples as it learns the underlying pattern present in the dataset.

Finally, the most crucial is the number of available samples in the dataset. Dataset's cardinality has a direct impact on the overall performance. Advanced deep learning model depends on a large dataset, a limited number of samples prevent us from applying complex very deep networks for table detection. A deep learning model built with limited data suffers from overfitting and poor inference time results.

To address these problems, we have gathered a new large-scale benchmark dataset for table detection. The presented dataset consists of 7K image samples from diverse sources capturing a wide variety of table occurrences. We have collected table samples from scanned documents, word documents, and searchable pdf documents. Collected samples were checked for quality standards by removing blurry, noisy, and low-quality samples from the final dataset.

As another contribution, we also provide baseline results using a deep learning-based model and classical selective search method. Additionally, we also provide a novel method to compute the diversity of the samples of a dataset by leveraging latent representation computed using a pre-trained

encoder.

The presented dataset can help the researchers to develop a novel table detection method to understand and map document layouts for information extraction. This dataset will make it easy for the community to apply data-dependent algorithms such as deep convolutional neural networks for the task of layout and table detection.

Our experimental results using the presented deep learning method show promising results in detecting complex table structures. The baseline results were able to outperform the classical computer vision-based methods for detecting tables asserting the advantages of a data-driven deep neural network.

The rest of the paper is organized as follows: Section 2 explores the current table detection methods and benchmarks. Section 3 introduces the presented dataset, its properties, and evaluation metrics. Section 4 presents the deep convolutional layer-based RetinaNet method and selective search-based detection method for table detection in the wild images. Section 5 shows the experimental results obtained by classical computer vision methods alongside the proposed deep learning method on our benchmark, and section 6 concludes the paper.

## II. RELATED WORK

In this section, we will go through the publicly available table detection datasets and the recent advancements of deep learning in this domain.

### A. Table Detection Datasets

TableBank [7] dataset is prepared from word and latex documents available on the internet. This dataset contains 417K labeled table images. This dataset does not contain any tables from scanned pdf documents. Another limitation is the diversity of the samples, this dataset was collected from '.docx' format documents and scientific articles from the arxiv.org website.

Marmot [8] dataset is consisting of 2000 pdf pages with tables. Most of these examples were collected from research papers.

ICDAR 2013 [9] dataset released as part of 2013 competition for both table detection and its structural analysis. It contains 128 samples collected mostly from US and EU government sources.

UNLV [10] dataset contains 427 samples collected from scanned documents. These samples were sourced from magazines, newspapers, corporate reports, business letters, etc.

DeepFigures [11] is a large dataset consisting of figures and tables samples. This dataset is collected from latex and XML sources. It has 1.4M induced tables, but it does not contain any scanned documents, also the intra-samples diversity of this dataset is limited.

To summarize our dataset has many advantages over the existing public datasets as follows:

- Samples include scanned and searchable documents.
- High diversity of samples, capturing a wide range of table designs.
- High resolution of samples.
- Biggest dataset with manual annotation.

### B. Table Detection Methods

Both classical computer vision and deep learning-based methods are used to solve the table detection problem. Recently convolutional detection-based methods achieved state-of-the-art results on publicly available datasets such as TableBank, ICDAR, Marmot, etc.

Li et al. [7] proposed a Faster-RCNN [12] based convolutional detection method and reported a performance of 0.93 F1 score in the TableBank dataset. They have used Resnet-101 and Resnet-152 very deep neural networks as feature extractor backbone.

TableNet [13] is another deep learning method formulate table detection as region segmentation problem and uses FCN architecture [14] to segment table region. It uses VGG-16 [15] as feature extractor for the FCN model. TableNet has reported a performance of 0.95 F1 score on the iCDAR dataset.

Another Faster-RCNN based approach proposed by Gilani et al. [16] reported state-of-the-art performance on the UNLV dataset.

Schreiber et al. [17] uses a deep learning-based method to detect tables and identify table structure by detecting rows, columns, and table cells. It also uses the Faster-RCNN method with VGG-16 as the feature extractor backbone.

Classical feature engineering approaches were also used to detect tables in scanned and searchable documents. Kasar et al. [18] used an SVM classifier on features extracted using horizontal and vertical lines information to predict if a sample has a table or not. Silva et al. [19] uses Hidden Markov model to detect tables from documents. Based on the MXY tree data structure Cesarini et al. [20] presented a hierarchical representation for locating tables in document images.

Despite the successes of applying deep learning models on various datasets, these methods still lack generalization performance on out-of-domain samples due to the constrained nature of the available public datasets. Applying these models to production scenarios is still a work in progress.

## III. THE DATASET

In this section, we introduce the metadata details and the evaluation criteria of STDW table detection dataset. Dataset can be accessed in this link: <https://github.com/subex/STDW>.

### A. The STDW Table Detection Dataset

**Data Sources:** To prepare the dataset, we have utilized the resources available on the internet. Documents containing tables were collected from various sources to ensure intra-dataset samples diversity. Sources such as electronic component datasheets, material safety data sheets, product safety data sheets, billing invoices, research papers, finance reports, books, etc are used for gathering the samples. Samples contain English, German, Japanese, Hindi, and many other languages capturing diverse scripts. Figure 2 shows some sample images from the collected dataset.

**Data Modalities:** Both scanned and searchable documents with tables are included in the dataset. Scanned documents include RGB and grayscale samples. Collected samples have

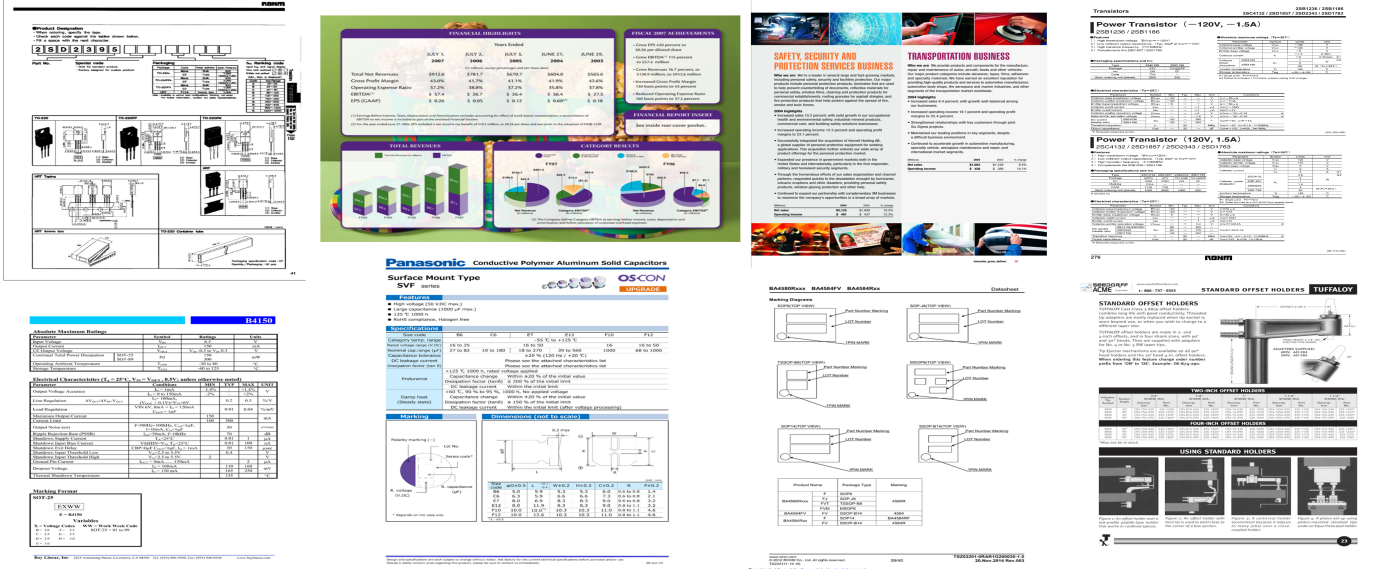


Fig. 2. Dataset samples images with diverse examples

one or more tables in them. Samples resolution varies from  $500 \times 500 \times 3$  to  $5000 \times 5000 \times 3$ , capturing a wide range of image qualities.

**Labelling:** All samples in the dataset are labeled manually using the GUI-based Labelme [21] annotation tool. Bounding box-based standard detection problem's labeling method is used to label all the images. For each of the image bounding boxes, coordinates are stored in an XML file as shown in the Listing 1 following the PASCAL VOC [22] annotation format. For each bounding box, top left  $(x_{min}, y_{min})$  and bottom-right  $(x_{max}, y_{max})$  coordinates are stored. Figure 3 shows a sample image with a bounding box marked on the image showing the position respective coordinates.

**Data Statistics:** Table I depicts the STDW dataset samples statistics.

## B. Benchmark Evaluations

We define criteria for two types of table detection evaluation metrics to unify reported results on this dataset. Work derived using this benchmark dataset may use these metrics for fair comparisons. We report the performance of the baseline models on these two metrics.

**IoU-Intersection over union:** Overlap between two bounding boxes is measured using Intersection Over Union (IoU) also known as Jaccard Index. We use this metric to measure the extent of the correctness of the predicted bounding box with the ground truth bounding box. Eq 1 shows the mathematical formulation on how to calculate IoU between two bounding boxes B1 and B2.

$$IoU = \frac{|B1 \cap B2|}{|B1 \cup B2|} \quad (1)$$

**AP-Average Precision:** Average Precision (AP) summarizes a precision-recall curve as the weighted mean of the

KD1084 SERIES					
ELECTRICAL CHARACTERISTICS OF KD1084A15 ( $V_I=4.5V$ , $C_I=C_O=10\mu F$ (Tant.), $T_A=-40$ to $+125^\circ C$ , unless otherwise specified)					
Symbol	Parameter	Test Conditions	Min.	Typ.	Max. Unit
$V_O$	Output Voltage	$I_O = 0mA$ , $T_J = 25^\circ C$	1.485	1.5	1.515 V
		$I_O = 0$ to $5A$ , $V_I = 3.1$ to $10V$ , $T_J = 25^\circ C$	1.47	1.5	1.53 V
$\Delta V_O$	Line Regulation	$I_O = 0mA$ , $V_I = 3.1$ to $10V$ , $T_J = 25^\circ C$	0.5	6	mV
		$I_O = 0$ to $5A$ , $V_I = 3.1$ to $10V$ , $T_J = 25^\circ C$	1	6	mV
$\Delta V_O$	Load Regulation	$I_O = 0$ to $5A$ , $T_J = 25^\circ C$	3	15	mV
$V_{dL}$	Dropout Voltage	$I_O = 0$ to $5A$	7	20	V
$I_Q$	Quiescent Current	$V_I = 10V$	5	10	mA
$I_{sc}$	Short Circuit Current	$V_I = V_O = 5V$	5.5	7	A
	Thermal Regulation	$T_A = 25^\circ C$ , 30ms pulse	0.003	0.015	%/W
SVR	Supply Voltage Rejection	$f = 120Hz$ , $C_O = 25\mu F$ , $I_O = 5A$ , $V_I = 5.3 \pm 1.5V$	60	75	dB
nN	RMS Output Noise Voltage (% of $V_O$ )	$T_A = 25^\circ C$ , $f = 10Hz$ to $100kHz$	0.003		%
S	Temperature Stability		0.5		%
S	Long Term Stability	$T_A = 125^\circ C$ , 1000Hrs	0.5		%

ELECTRICAL CHARACTERISTICS OF KD1084A18 ( $V_I=4.8V$ , $C_I=C_O=10\mu F$ (Tant.), $T_A=-40$ to $+125^\circ C$ , unless otherwise specified)					
Symbol	Parameter	Test Conditions	Min.	Typ.	Max. Unit
$V_O$	Output Voltage	$I_O = 0mA$ , $T_J = 25^\circ C$	1.782	1.8	1.818 V
		$I_O = 0$ to $5A$ , $V_I = 3.4$ to $10V$ , $T_J = 25^\circ C$	1.764	1.8	1.836 V
$\Delta V_O$	Line Regulation	$I_O = 0mA$ , $V_I = 3.4$ to $10V$ , $T_J = 25^\circ C$	0.5	6	mV
		$I_O = 0$ to $5A$ , $V_I = 3.4$ to $10V$ , $T_J = 25^\circ C$	1	6	mV
$\Delta V_O$	Load Regulation	$I_O = 0$ to $5A$ , $T_J = 25^\circ C$	3	15	mV
$V_{dL}$	Dropout Voltage	$I_O = 5A$	7	20	V
$I_Q$	Quiescent Current	$V_I = 10V$	5	10	mA
$I_{sc}$	Short Circuit Current	$V_I = V_O = 5V$	5.5	7	A
	Thermal Regulation	$T_A = 25^\circ C$ , 30ms pulse	0.003	0.015	%/W
SVR	Supply Voltage Rejection	$f = 120Hz$ , $C_O = 25\mu F$ , $I_O = 5A$ , $V_I = 5.3 \pm 1.5V$	60	75	dB
nN	RMS Output Noise Voltage (% of $V_O$ )	$T_A = 25^\circ C$ , $f = 10Hz$ to $100kHz$	0.003		%
S	Temperature Stability		0.5		%
S	Long Term Stability	$T_A = 125^\circ C$ , 1000Hrs	0.5		%

Fig. 3. An example image with bounding boxes annotation. We denote top-left corner as  $(x_{min}, y_{min})$  and bottom-right corner as  $(x_{max}, y_{max})$

precisions obtained at the different thresholds. The increase in recall from the previous threshold has used a weight. Eq 2 shows the mathematical formulation on how to compute AP using a precision-recall curve, where  $P_n$  and  $R_n$  are the precision and recall at the  $n$ th threshold.

$$AP = \sum_n (R_n - R_{n-1}) P_n \quad (2)$$

AP metric is calculated at different IoU thresholds to get

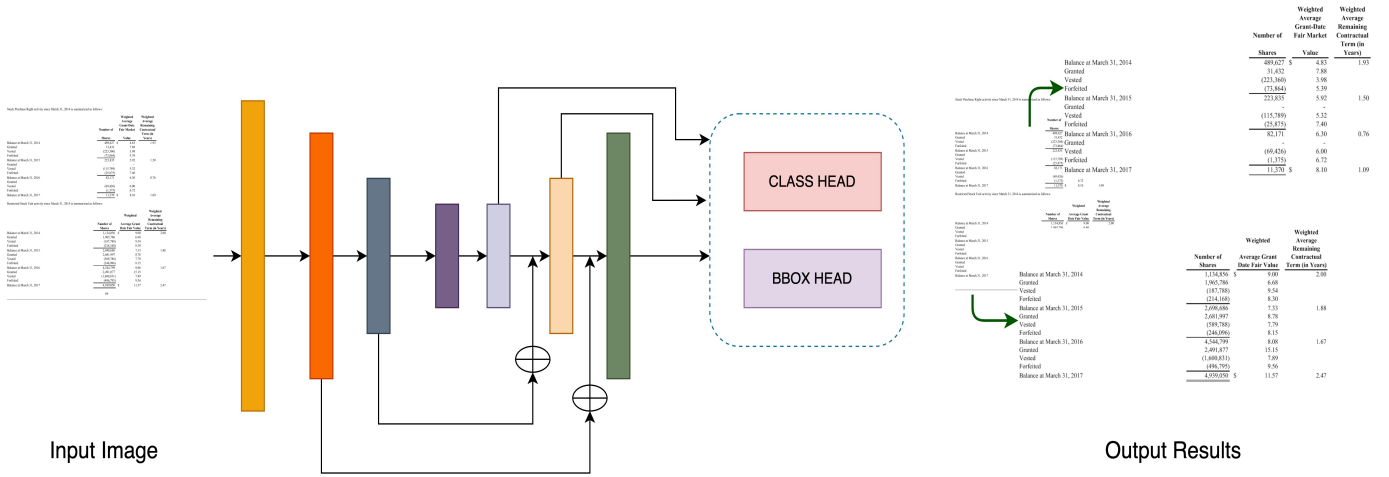


Fig. 4. RetinaNet based method for Table Detection. RetinaNet uses two task-specific heads, one for predicting objects labels and the other for predicting object bounding boxes. RetinaNet is a fully convolutional model and it uses upsampling layers and skip connections to build the input layers for the task-specific heads.

Listing 1. An example XML file content showing the annotation for a single bounding box.

```
<annotation>
  <object>
    <name>Table</name>
    <pose>Unspecified</pose>
    <truncated>0</truncated>
    <difficult>0</difficult>
    <bndbox>
      <xmin>541</xmin>
      <ymin>970</ymin>
      <xmax>4060</xmax>
      <ymax>2766</ymax>
    </bndbox>
  </object>
  ...
  <object>
    ...
  </object>
</annotation>
```

STDW	No of Images	No of Tables
Scanned PDFs	2345	5102
Searchable documents	4945	7329

TABLE I

STDW DATASET SAMPLES STATISTICS. IT INCLUDES BOTH SCANNED AND SEARCHABLE/NATIVE-DIGITAL DOCUMENTS,

the best combination of IoU and AP for the object detection task.

#### IV. METHODS

In this section, we detail a data-driven deep learning method and a classical feature-based method to locate the table in

images. We formulate the problem as a classic object detection problem, where the object of consideration will be a tabular structure present in the images.

Deep learning-based object detection methods are proven to be very effective. We use RetinaNet [23] object detection method as baseline for this dataset. RetinaNet achieved state-of-the-art performance on the COCO [24] dataset. We also use a selective search [25] model for object detection to report baseline results using classical computer vision.

In this section, we introduce the deep convolutional object detection method RetinaNet and the selective search-based objection detection method.

##### A. RetinaNet for Table Detection

RetinaNet is a one-stage, dense objective detection method designed using convolutional layers. It consists of a backbone network and two task-specific heads. The backbone network is designed to model input image features using convolutional layers. The backbone network is a stack of multiple skip connection-based convolutional blocks. Task-specific heads are designed to get classification scores and the coordinates for each of the anchor bounding boxes. Figure 4 shows a high-level depiction of the RetinaNet. RetinaNet addresses the extreme foreground-background class imbalance problem observed in the object detector training by introducing a sample complexity-based weighted cross-entropy loss called focal loss. Focal loss enforces the trainer to focus on hard examples by assigning higher weights. Cross entropy loss for binary classification is defined as shown in the Eq 3

$$CE(p, y) = \begin{cases} -\log(p) & \text{if } y = 1 \\ -\log(1 - p) & \text{otherwise} \end{cases} \quad (3)$$

To handle the large class imbalance problem focal loss adds a modulating factor  $(1 - p_t)^\lambda$  to the original binary cross entropy loss function. Focal loss is defined as shown in the Eq 4, where  $\lambda \geq 0$  is a tuneable parameter.



Datasets	Samples	Diversity	Annotation Method	Modalities
ICDAR 2013	128	805.79	Manual	Searchable PDFs
TableBank	417,234	755.32	XML + Latex	Word and Latex documents
Marmot	2000	608.65	Manual	Searchable PDFs
UNLV	427	-	Manual	Scanned documents
DeepFigures	1.4M	-	XML + Latex	Word and Latex documents
<b>STDW (ours)</b>	7294	<b>900.72</b>	Manual	Searchable PDFs and Scanned documents

TABLE II

COMPARISONS BETWEEN THE STDW DATASET AND SOME OF THE OTHER PUBLICLY AVAILABLE DATASETS FOR TABLE DETECTION. OUR DATASET PROVIDES THE MOST DIVERSE, HIGH-QUALITY SAMPLES.

$$FL(p_t) = -(1 - p)^\lambda \log(p_t) \quad (4)$$

In this work we use a  $\alpha$ -balanced variant of the focal loss as shown in the Eq 5

$$FL(p_t) = -\alpha_t(1 - p)^\lambda \log(p_t) \quad (5)$$

### B. Selective Search

Selective search is a method to detect all possible object bounding boxes in an input image. Selective search is combined with classical image-level features and a support vector machine to detect objects. It uses a hierarchical grouping algorithm to find all possible bounding boxes with an object, those bounding boxes can be overlapping. Selective search assigns objectness score to bounding boxes denoting the probability of object presence inside the bounding box. A bounding box with a high objectness score might contain the object of interest. For computing features of bounding boxes bag-of-words [26] with color-SIFT descriptors [27] is used. For the classification of bounding boxes, a support vector machine with a histogram intersection kernel is used.

### C. Dataset Diversity

We estimate diversity based on the dataset's sample variations in the latent space. The spread of the dataset in the latent space is defined as diversity. The larger the spread of the samples, the higher is the diversity. To calculate the latent representation of each of the samples we use an ImageNet [28] pre-trained VGG-16 [15] model's *block5\_pool* layer. VGG-16 is a very deep convolutional model used for image-related problems. The latent representation is of dimension 25088 and computed on input image resized to [224, 224, 3]. Algorithm 1 provides the full procedure for diversity computation using a deep convolutional encoder model.

## V. EXPERIMENTS

In our experiments, we evaluate the classical computer vision method and convolutional RetinaNet model on our dataset.

We have used Tensorflow [29] and Datum [30] for deep learning experiments described in this work. Tensorflow is used to build and train the RetinaNet model and Datum is used to prepare and load the dataset for training. Batch normalization [31] is used to reduce covariate shift and achieve faster convergence. Also, we have used the Nesterov momentum

### Algorithm 1 Dataset Diversity Metric

```

1: Initialize VGG-16 model with ImageNet weights.
2:  $features \leftarrow []$ 
3: // Compute samples latent representations
4: for each image  $image\_filepath$  do
5:   // Read, resize and normalize image
6:    $image\_np = read\_image(image\_filepath)$ 
7:    $image\_np = resize\_and\_normalize(image\_np)$ 
8:   // Compute latent representation
9:    $feature = VGG16(image\_np)$ 
10:   $features \leftarrow features \cup feature$ 
11: // Compute standard deviation across features dimension
12:  $features\_std \leftarrow compute\_std(features, axis = 1)$ 
13: // Compute L2 norm
14:  $diversity = ||features\_std||_2$ 

```

Method	IOU	AP
RetinaNet	0.5	0.78
Selective Search	0.5	0.61

TABLE III

PERFORMANCE OF CLASSICAL AND DEEP LEARNING METHODS ON STDW

optimizer with a constant learning rate. RetinaNet model is trained using a GPU accelerator for 30 epochs to reach the baseline performance as reported in Table III. For selective search, we use the official Matlab code provided by the author.

### A. Baseline results for STDW

We provide baseline results for table detection on the STDW dataset using two methods. In one method we use the deep learning-based RetinaNet model and in the other method, we use a selective search-based object detection approach. For baseline results, IOU and AP are computed on the test set. We trained a RetinaNet model with XX feature extractor for detecting tables from input images. The hyperparameter set used in the RetinaNet experiment is shown in Table IV. For a selective search-based approach we use a visual codebook of size 4000 and 4 levels spatial pyramid using a  $1 \times 1$ ,  $2 \times 2$ ,  $3 \times 3$  and  $4 \times 4$  division. This setting results in a total feature vector of length 360000.

Table III shows the baseline results obtained using the deep learning-based RetinaNet model and classical selective search-based approach. RetinaNet performed significantly higher than

**ELECTRICAL CHARACTERISTICS**

The electrical characteristics of a SMT50 device are similar to that of a self-gated triac, but the SMT50 is a true terminal device with no gate. The gate function is achieved by an external current controlled mechanism.

Like the T-VS device, the SMT50 has a standoff voltage (V<sub>RM</sub>) which should be equal to or greater than the operating voltage of the system to be protected. At this voltage (V<sub>RM</sub>) the current consumption of the SMT50 is negligible and will not affect the protected system.

When a transient occurs, the voltage across the SMT50 will increase until the breakdown voltage (V<sub>BR</sub>) is reached. At this point the device will operate in a similar way to a T-VS device and is in avalanche mode.

The voltage of the transient will now be limited and will only increase by a few volts as the device diverts more current. As the transient current rises, a level of current through the device is reached (I<sub>HT</sub>) which causes the device to switch to a fully conductive state such that the voltage across the device is now only a few volts (V<sub>CE</sub>). The voltage at which the device switches from the avalanche mode to the fully conductive state (V<sub>CE</sub>) is known as the Breakover voltage (V<sub>BO</sub>). When the device is in the V<sub>CE</sub> state, high currents can be diverted without damage to the SMT50 due to the low voltage across the device, since the limiting factor in such devices is dissipated power (V × I).

Resetting of the device to the non-conducting state is controlled by the current flowing through the device. When the current falls below a certain value, known as the Holding Current (I<sub>H</sub>), the device resets automatically.

As with the avalanche T-VS device, if the SMT50 is subjected to a surge current which is beyond its maximum rating, then the device will fail in short circuit mode, ensuring that the equipment is ultimately protected.

**SELECTING A SMT50**

- When selecting a SMT50 device, it is important that the V<sub>RM</sub> of the device is equal to or greater than the operating voltage of the system.
- The minimum Holding Current (I<sub>H</sub>) must be greater than the current the system is capable of detecting otherwise the device will remain conducting following a transient condition.

**Table: 99-07**

COMPLIES WITH THE FOLLOWING STANDARDS	PEAK SURGE VOLTAGE	STANDOFF VOLTAGE	CURRENT VOLTAGE	ADMISSIBLE SP	NECESSARY RESISTOR
EC-ETC (UL-609)	1000	10-100	5-100	25	100
EC-ETC (UL-147)	1000	10-100	5-100	25	100
UL-609A1	1000	10-100	5-100	25	100
UL-609A2	1000	10-100	5-100	25	100
UL-609A3	1000	10-100	5-100	25	100
UL-609A4	1000	10-100	5-100	25	100
UL-609A5	1000	10-100	5-100	25	100
UL-609A6	1000	10-100	5-100	25	100
UL-609A7	1000	10-100	5-100	25	100
UL-609A8	1000	10-100	5-100	25	100
UL-609A9	1000	10-100	5-100	25	100
UL-609A10	1000	10-100	5-100	25	100
UL-609A11	1000	10-100	5-100	25	100
UL-609A12	1000	10-100	5-100	25	100
UL-609A13	1000	10-100	5-100	25	100
UL-609A14	1000	10-100	5-100	25	100
UL-609A15	1000	10-100	5-100	25	100
UL-609A16	1000	10-100	5-100	25	100
UL-609A17	1000	10-100	5-100	25	100
UL-609A18	1000	10-100	5-100	25	100
UL-609A19	1000	10-100	5-100	25	100
UL-609A20	1000	10-100	5-100	25	100
UL-609A21	1000	10-100	5-100	25	100
UL-609A22	1000	10-100	5-100	25	100
UL-609A23	1000	10-100	5-100	25	100
UL-609A24	1000	10-100	5-100	25	100
UL-609A25	1000	10-100	5-100	25	100
UL-609A26	1000	10-100	5-100	25	100
UL-609A27	1000	10-100	5-100	25	100
UL-609A28	1000	10-100	5-100	25	100
UL-609A29	1000	10-100	5-100	25	100
UL-609A30	1000	10-100	5-100	25	100
UL-609A31	1000	10-100	5-100	25	100
UL-609A32	1000	10-100	5-100	25	100
UL-609A33	1000	10-100	5-100	25	100
UL-609A34	1000	10-100	5-100	25	100
UL-609A35	1000	10-100	5-100	25	100
UL-609A36	1000	10-100	5-100	25	100
UL-609A37	1000	10-100	5-100	25	100
UL-609A38	1000	10-100	5-100	25	100
UL-609A39	1000	10-100	5-100	25	100
UL-609A40	1000	10-100	5-100	25	100
UL-609A41	1000	10-100	5-100	25	100
UL-609A42	1000	10-100	5-100	25	100
UL-609A43	1000	10-100	5-100	25	100
UL-609A44	1000	10-100	5-100	25	100
UL-609A45	1000	10-100	5-100	25	100
UL-609A46	1000	10-100	5-100	25	100
UL-609A47	1000	10-100	5-100	25	100
UL-609A48	1000	10-100	5-100	25	100
UL-609A49	1000	10-100	5-100	25	100
UL-609A50	1000	10-100	5-100	25	100
UL-609A51	1000	10-100	5-100	25	100
UL-609A52	1000	10-100	5-100	25	100
UL-609A53	1000	10-100	5-100	25	100
UL-609A54	1000	10-100	5-100	25	100
UL-609A55	1000	10-100	5-100	25	100
UL-609A56	1000	10-100	5-100	25	100
UL-609A57	1000	10-100	5-100	25	100
UL-609A58	1000	10-100	5-100	25	100
UL-609A59	1000	10-100	5-100	25	100
UL-609A60	1000	10-100	5-100	25	100
UL-609A61	1000	10-100	5-100	25	100
UL-609A62	1000	10-100	5-100	25	100
UL-609A63	1000	10-100	5-100	25	100
UL-609A64	1000	10-100	5-100	25	100
UL-609A65	1000	10-100	5-100	25	100
UL-609A66	1000	10-100	5-100	25	100
UL-609A67	1000	10-100	5-100	25	100
UL-609A68	1000	10-100	5-100	25	100
UL-609A69	1000	10-100	5-100	25	100
UL-609A70	1000	10-100	5-100	25	100
UL-609A71	1000	10-100	5-100	25	100
UL-609A72	1000	10-100	5-100	25	100
UL-609A73	1000	10-100	5-100	25	100
UL-609A74	1000	10-100	5-100	25	100
UL-609A75	1000	10-100	5-100	25	100
UL-609A76	1000	10-100	5-100	25	100
UL-609A77	1000	10-100	5-100	25	100
UL-609A78	1000	10-100	5-100	25	100
UL-609A79	1000	10-100	5-100	25	100
UL-609A80	1000	10-100	5-100	25	100
UL-609A81	1000	10-100	5-100	25	100
UL-609A82	1000	10-100	5-100	25	100
UL-609A83	1000	10-100	5-100	25	100
UL-609A84	1000	10-100	5-100	25	100
UL-609A85	1000	10-100	5-100	25	100
UL-609A86	1000	10-100	5-100	25	100
UL-609A87	1000	10-100	5-100	25	100
UL-609A88	1000	10-100	5-100	25	100
UL-609A89	1000	10-100	5-100	25	100
UL-609A90	1000	10-100	5-100	25	100
UL-609A91	1000	10-100	5-100	25	100
UL-609A92	1000	10-100	5-100	25	100
UL-609A93	1000	10-100	5-100	25	100
UL-609A94	1000	10-100	5-100	25	100
UL-609A95	1000	10-100	5-100	25	100
UL-609A96	1000	10-100	5-100	25	100
UL-609A97	1000	10-100	5-100	25	100
UL-609A98	1000	10-100	5-100	25	100
UL-609A99	1000	10-100	5-100	25	100
UL-609A100	1000	10-100	5-100	25	100

**FEATURES**

- 1. 16-CHARACTER WITH CURSOR
- BUILT-IN CONTROLLER IC
- 1 V POWER SUPPLY
- 1.0 MHz CRYSTAL

**MECHANICAL DATA**

ITEM	DESCRIPTION	UNIT
1	Module Size (W x H x L)	12.7 x 12.7 x 12.7 mm
2	Module Size (W x H x L)	12.7 x 12.7 x 12.7 mm
3	Module Size (W x H x L)	12.7 x 12.7 x 12.7 mm
4	Module Size (W x H x L)	12.7 x 12.7 x 12.7 mm
5	Module Size (W x H x L)	12.7 x 12.7 x 12.7 mm
6	Module Size (W x H x L)	12.7 x 12.7 x 12.7 mm
7	Module Size (W x H x L)	12.7 x 12.7 x 12.7 mm
8	Module Size (W x H x L)	12.7 x 12.7 x 12.7 mm
9	Module Size (W x H x L)	12.7 x 12.7 x 12.7 mm
10	Module Size (W x H x L)	12.7 x 12.7 x 12.7 mm
11	Module Size (W x H x L)	12.7 x 12.7 x 12.7 mm
12	Module Size (W x H x L)	12.7 x 12.7 x 12.7 mm
13	Module Size (W x H x L)	12.7 x 12.7 x 12.7 mm
14	Module Size (W x H x L)	12.7 x 12.7 x 12.7 mm
15	Module Size (W x H x L)	12.7 x 12.7 x 12.7 mm
16	Module Size (W x H x L)	12.7 x 12.7 x 12.7 mm
17	Module Size (W x H x L)	12.7 x 12.7 x 12.7 mm
18	Module Size (W x H x L)	12.7 x 12.7 x 12.7 mm
19	Module Size (W x H x L)	12.7 x 12.7 x 12.7 mm
20	Module Size (W x H x L)	12.7 x 12.7 x 12.7 mm
21	Module Size (W x H x L)	12.7 x 12.7 x 12.7 mm
22	Module Size (W x H x L)	12.7 x 12.7 x 12.7 mm
23	Module Size (W x H x L)	12.7 x 12.7 x 12.7 mm
24	Module Size (W x H x L)	12.7 x 12.7 x 12.7 mm
25	Module Size (W x H x L)	12.7 x 12.7 x 12.7 mm
26	Module Size (W x H x L)	12.7 x 12.7 x 12.7 mm
27	Module Size (W x H x L)	12.7 x 12.7 x 12.7 mm
28	Module Size (W x H x L)	12.7 x 12.7 x 12.7 mm
29	Module Size (W x H x L)	12.7 x 12.7 x 12.7 mm
30	Module Size (W x H x L)	12.7 x 12.7 x 12.7 mm
31	Module Size (W x H x L)	12.7 x 12.7 x 12.7 mm
32	Module Size (W x H x L)	12.7 x 12.7 x 12.7 mm
33	Module Size (W x H x L)	12.7 x 12.7 x 12.7 mm
34	Module Size (W x H x L)	12.7 x 12.7 x 12.7 mm
35	Module Size (W x H x L)	12.7 x 12.7 x 12.7 mm
36	Module Size (W x H x L)	12.7 x 12.7 x 12.7 mm
37	Module Size (W x H x L)	12.7 x 12.7 x 12.7 mm
38	Module Size (W x H x L)	12.7 x 12.7 x 12.7 mm
39	Module Size (W x H x L)	12.7 x 12.7 x 12.7 mm
40	Module Size (W x H x L)	12.7 x 12.7 x 12.7 mm
41	Module Size (W x H x L)	12.7 x 12.7 x 12.7 mm
42	Module Size (W x H x L)	12.7 x 12.7 x 12.7 mm
43	Module Size (W x H x L)	12.7 x 12.7 x 12.7 mm
44	Module Size (W x H x L)	12.7 x 12.7 x 12.7 mm
45	Module Size (W x H x L)	12.7 x 12.7 x 12.7 mm
46	Module Size (W x H x L)	12.7 x 12.7 x 12.7 mm
47	Module Size (W x H x L)	12.7 x 12.7 x 12.7 mm
48	Module Size (W x H x L)	12.7 x 12.7 x 12.7 mm
49	Module Size (W x H x L)	12.7 x 12.7 x 12.7 mm
50	Module Size (W x H x L)	12.7 x 12.7 x 12.7 mm
51	Module Size (W x H x L)	12.7 x 12.7 x 12.7 mm
52	Module Size (W x H x L)	12.7 x 12.7 x 12.7 mm
53	Module Size (W x H x L)	12.7 x 12.7 x 12.7 mm
54	Module Size (W x H x L)	12.7 x 12.7 x 12.7 mm
55	Module Size (W x H x L)	12.7 x 12.7 x 12.7 mm
56	Module Size (W x H x L)	12.7 x 12.7 x 12.7 mm
57	Module Size (W x H x L)	12.7 x 12.7 x 12.7 mm
58	Module Size (W x H x L)	12.7 x 12.7 x 12.7 mm
59	Module Size (W x H x L)	12.7 x 12.7 x 12.7 mm
60	Module Size (W x H x L)	12.7 x 12.7 x 12.7 mm
61	Module Size (W x H x L)	12.7 x 12.7 x 12.7 mm
62	Module Size (W x H x L)	12.7 x 12.7 x 12.7 mm
63	Module Size (W x H x L)	12.7 x 12.7 x 12.7 mm
64	Module Size (W x H x L)	12.7 x 12.7 x 12.7 mm
65	Module Size (W x H x L)	12.7 x 12.7 x 12.7 mm
66	Module Size (W x H x L)	12.7 x 12.7 x 12.7 mm
67	Module Size (W x H x L)	12.7 x 12.7 x 12.7 mm
68	Module Size (W x H x L)	12.7 x 12.7 x 12.7 mm
69	Module Size (W x H x L)	12.7 x 12.7 x 12.7 mm
70	Module Size (W x H x L)	12.7 x 12.7 x 12.7 mm
71	Module Size (W x H x L)	12.7 x 12.7 x 12.7 mm
72	Module Size (W x H x L)	12.7 x 12.7 x 12.7 mm
73	Module Size (W x H x L)	12.7 x 12.7 x 12.7 mm
74	Module Size (W x H x L)	12.7 x 12.7 x 12.7 mm
75	Module Size (W x H x L)	12.7 x 12.7 x 12.7 mm
76	Module Size (W x H x L)	12.7 x 12.7 x 12.7 mm
77	Module Size (W x H x L)	12.7 x 12.7 x 12.7 mm
78	Module Size (W x H x L)	12.7 x 12.7 x 12.7 mm
79	Module Size (W x H x L)	12.7 x 12.7 x 12.7 mm
80	Module Size (W x H x L)	12.7 x 12.7 x 12.

- [3] M. Haloi, "Rethinking convolutional semantic segmentation learning," *arXiv preprint arXiv:1710.07991*, 2017.
- [4] A. Krizhevsky, I. Sutskever, and G. E. Hinton, "Imagenet classification with deep convolutional neural networks," *Advances in neural information processing systems*, vol. 25, pp. 1097–1105, 2012.
- [5] M. Haloi, "Deep learning: Generalization requires deep compositional feature space design," *arXiv preprint arXiv:1706.01983*, 2017.
- [6] K. He, G. Gkioxari, P. Dollár, and R. Girshick, "Mask r-cnn," in *Proceedings of the IEEE international conference on computer vision*, 2017, pp. 2961–2969.
- [7] M. Li, L. Cui, S. Huang, F. Wei, M. Zhou, and Z. Li, "Tablebank: A benchmark dataset for table detection and recognition," *arXiv preprint arXiv:1903.01949*, 2019.
- [8] J. Fang, X. Tao, Z. Tang, R. Qiu, and Y. Liu, "Dataset, ground-truth and performance metrics for table detection evaluation," in *2012 10th IAPR International Workshop on Document Analysis Systems*. IEEE, 2012, pp. 445–449.
- [9] M. Göbel, T. Hassan, E. Oro, and G. Orsi, "Icdar 2013 table competition," in *2013 12th International Conference on Document Analysis and Recognition*. IEEE, 2013, pp. 1449–1453.
- [10] A. Shahab, F. Shafait, T. Kieninger, and A. Dengel, "An open approach towards the benchmarking of table structure recognition systems," in *Proceedings of the 9th IAPR International Workshop on Document Analysis Systems*, 2010, pp. 113–120.
- [11] N. Siegel, N. Lourie, R. Power, and W. Ammar, "Extracting scientific figures with distantly supervised neural networks," in *Proceedings of the 18th ACM/IEEE on joint conference on digital libraries*, 2018, pp. 223–232.
- [12] S. Ren, K. He, R. Girshick, and J. Sun, "Faster r-cnn: Towards real-time object detection with region proposal networks," *Advances in neural information processing systems*, vol. 28, pp. 91–99, 2015.
- [13] S. S. Paliwal, D. Vishwanath, R. Rahul, M. Sharma, and L. Vig, "Tablenet: Deep learning model for end-to-end table detection and tabular data extraction from scanned document images," in *2019 International Conference on Document Analysis and Recognition (ICDAR)*. IEEE, 2019, pp. 128–133.
- [14] J. Long, E. Shelhamer, and T. Darrell, "Fully convolutional networks for semantic segmentation," in *Proceedings of the IEEE conference on computer vision and pattern recognition*, 2015, pp. 3431–3440.
- [15] K. Simonyan and A. Zisserman, "Very deep convolutional networks for large-scale image recognition," *arXiv preprint arXiv:1409.1556*, 2014.
- [16] A. Gilani, S. R. Qasim, I. Malik, and F. Shafait, "Table detection using deep learning," in *2017 14th IAPR international conference on document analysis and recognition (ICDAR)*, vol. 1. IEEE, 2017, pp. 771–776.
- [17] S. Schreiber, S. Agne, I. Wolf, A. Dengel, and S. Ahmed, "Deepdesrt: Deep learning for detection and structure recognition of tables in document images," in *2017 14th IAPR international conference on document analysis and recognition (ICDAR)*, vol. 1. IEEE, 2017, pp. 1162–1167.
- [18] T. Kasar, P. Barlas, S. Adam, C. Chatelain, and T. Paquet, "Learning to detect tables in scanned document images using line information," in *2013 12th International Conference on Document Analysis and Recognition*. IEEE, 2013, pp. 1185–1189.
- [19] A. C. e Silva, "Learning rich hidden markov models in document analysis: Table location," in *2009 10th International Conference on Document Analysis and Recognition*. IEEE, 2009, pp. 843–847.
- [20] F. Cesarini, S. Marinai, L. Sarti, and G. Soda, "Trainable table location in document images," in *Object recognition supported by user interaction for service robots*, vol. 3. IEEE, 2002, pp. 236–240.
- [21] K. Wada, "Labelme: Image polygonal annotation with python," *GitHub repository*, 2016.
- [22] M. Everingham and J. Winn, "The pascal visual object classes challenge 2012 (voc2012) development kit," *Pattern Analysis, Statistical Modelling and Computational Learning, Tech. Rep.*, vol. 8, p. 5, 2011.
- [23] T.-Y. Lin, P. Goyal, R. Girshick, K. He, and P. Dollár, "Focal loss for dense object detection," in *Proceedings of the IEEE international conference on computer vision*, 2017, pp. 2980–2988.
- [24] T.-Y. Lin, M. Maire, S. Belongie, J. Hays, P. Perona, D. Ramanan, P. Dollár, and C. L. Zitnick, "Microsoft coco: Common objects in context," in *European conference on computer vision*. Springer, 2014, pp. 740–755.
- [25] J. R. Uijlings, K. E. Van De Sande, T. Gevers, and A. W. Smeulders, "Selective search for object recognition," *International journal of computer vision*, vol. 104, no. 2, pp. 154–171, 2013.
- [26] G. Csurka, C. Dance, L. Fan, J. Willamowski, and C. Bray, "Visual categorization with bags of keypoints," in *Workshop on statistical learning in computer vision, ECCV*, vol. 1, no. 1-22. Prague, 2004, pp. 1–2.
- [27] K. Van De Sande, T. Gevers, and C. Snoek, "Evaluating color descriptors for object and scene recognition," *IEEE transactions on pattern analysis and machine intelligence*, vol. 32, no. 9, pp. 1582–1596, 2009.
- [28] O. Russakovsky, J. Deng, H. Su, J. Krause, S. Satheesh, S. Ma, Z. Huang, A. Karpathy, A. Khosla, M. Bernstein *et al.*, "Imagenet large scale visual recognition challenge," *International journal of computer vision*, vol. 115, no. 3, pp. 211–252, 2015.
- [29] M. Abadi, A. Agarwal, P. Barham, E. Brevdo, Z. Chen, C. Citro, G. S. Corrado, A. Davis, J. Dean, M. Devin *et al.*, "Tensorflow: Large-scale machine learning on heterogeneous distributed systems," *arXiv preprint arXiv:1603.04467*, 2016.
- [30] M. Haloi and S. Shekhar, "Datum: A system for tfrecord dataset management," *GitHub repository*, 2021.
- [31] S. Ioffe and C. Szegedy, "Batch normalization: Accelerating deep network training by reducing internal covariate shift," in *International conference on machine learning*. PMLR, 2015, pp. 448–456.